Automation and Robotics in Construction XVI © 1999 by UC3M

CONTROL OF HEAVY LOAD MANIPULATORS IN VARYING ENVIRONMENTS

Artur Komainda and Manfred Hiller

Gerhard-Mercator-Universität – GH Duisburg, Fachgebiet Mechatronik,
Lotharstraße 1, 47057 Duisburg, Germany
{komainda, hiller}@mechatronik.uni-duisburg.de

Abstract

The aim of this paper is to present concepts for the motion control of redundant manipulators in a changing environment. In order to be able to avoid collisions with unexpected and moving obstacles, an intelligent control concept is required which combines the off-line planned paths with on-line sensor information. Solutions for the combined collision free motion control of the redundant degrees of freedom (d.o.f.), and the degrees of freedom of the Tool Center Point (TCP) are presented. The redundant d.o.f. are influenced by nonlinear potential forces, which can be easy introduced into concepts for the inverse kinematics. Motion control (position and orientation) of the TCP is implemented with an artificial elastic band in the workspace of the TCP, which enables it to react to modifications in the environment.

Keywords: *Motion Control, Redundancy, Large-Scale Manipulators*

1 Introduction

Manipulation tasks such as repairing and inspecting bridges or high voltage transmission lines, cleaning the outsides of buildings (Fig. 1), or shifting piping require extreme mechanical properties, as well as complex motion control of the system. Redundant large scale manipulators fulfil these requirements, but the traditional motion control concepts are not sufficient. The control concepts investigated in this paper are applied to the redundant large scale manipulator [Wanner 1996] shown in Fig. 2. It is a combination of a six d.o.f. macro-manipulator for large scale motions and a six d.o.f. micro-manipulator for small scale motions (e.g. of a gripper or a brush). The macro-manipulator consists of five arm elements which are connected by parallel revolute joints, fixed to a base that rotates about a vertical axis. Since it is driven by hydraulic actuators acting over transmission linkage mechanisms, closed kinematic loops occur. The micro-manipulator however has the form of an open kinematic chain. All closed loops can be solved explicitly, and the vector of generalized coordinates can be denoted as:

$$q = [s_1, \ldots, s_6, \beta_1, \ldots, \beta_6]^T , \qquad (1)$$

where β_1 describes the rotation about the vertical axis and s_1 – s_5 are the displacements of the hydraulic actuators. To orientate the brush in the three dimensional workspace the angles of rotation β_2 to β_5 are used. Furthermore a linear actuator used for small displacements of the micro-manipulator is represented by s_6. The angle β_6 describes the rotation of the brush.

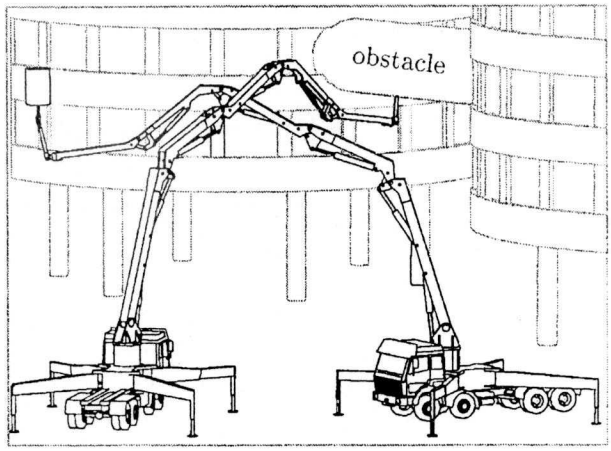

Figure 1: Manipulation Task

Thus, regarding end-effector position and orientation, six redundant degrees of freedom exist. The position and orientation parameters are represented by the vector $\boldsymbol{w}_{tcp} \in \mathbb{R}^n$, with $n = 6$. The relationship between the end-effector coordinates and the generalized coordinates $\boldsymbol{q} \in \mathbb{R}^f$, with $f = 12$, is:

$$\varphi_{tcp}(\boldsymbol{q}) = \boldsymbol{w}_{tcp} = [\boldsymbol{w}^T_{tcp,\,pos}, \boldsymbol{w}^T_{tcp,\,orient}]^T \qquad (2)$$

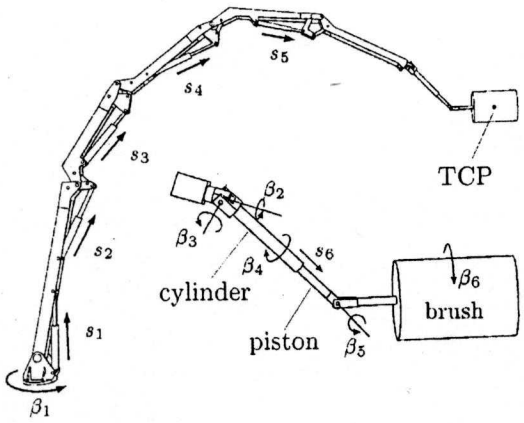

Figure 2: Macro-/Micro-manipulator

The model of the environment consists of obstacles that are created of primitive components (e. g. spheres, cylinders, right parallelepipeds or planes), which are combined in the three dimensional workspace to form complex obstacles. In this manner complex environments with buildings, trees and even overhead power lines can be constructed [Schneider et al. 1995]. With proximity sensors installed on the boom of the manipulator the vector representing the shortest distance between a sensor and an obstacle can be determined. This vector becomes important for collision avoidance, as is discussed in sections 2.1 and 3.1.

2 Motion Control of the Redundant Degrees of Freedom

Redundant systems are characterized by a degree of high mobility, which can be used for additional conditions. At first the problem of the inverse kinematics of redundant systems has to be solved with the method of Resolved Motion Control [Whitney 1969]. An appropriate linear system of equations for the inverse kinematics can be formulated as [Woernle 1993]:

$$\begin{bmatrix} \boldsymbol{P} & \boldsymbol{J}_{tcp}^T \\ \boldsymbol{J}_{tcp} & \boldsymbol{0} \end{bmatrix} \begin{bmatrix} \ddot{\boldsymbol{q}} \\ \boldsymbol{\lambda} \end{bmatrix} = \begin{bmatrix} \boldsymbol{p} \\ \ddot{\boldsymbol{w}}_{tcp} - \dot{\boldsymbol{J}}_{tcp}\,\dot{\boldsymbol{q}} \end{bmatrix}, \quad (3)$$

with the weighting matrix $\boldsymbol{P} \in \mathbb{R}^{f \times f}$, the weighting vector $\boldsymbol{p} \in \mathbb{R}^f$, the LAGRANGE-multipliers $\boldsymbol{\lambda}$ and the terms $\boldsymbol{J}_{tcp} = \frac{\partial \boldsymbol{\varphi}_{tcp}}{\partial \boldsymbol{q}}$ and $\dot{\boldsymbol{J}}_{tcp} = \frac{d}{dt}\boldsymbol{J}_{tcp}$.

2.1 Controlled Motion in Nullspace

An important property of redundant systems is given by their motion in the nullspace of TCP-motion. It enables to a reconfiguration of the boom, where the position and orientation of the TCP is not changed. This additional mobility is used for the consideration of natural constraints of the manipulator (e. g. joint limitations, max. and min. velocities, etc.) The matrix $\boldsymbol{P}$ and the vector $\boldsymbol{p}$ of (Eq. 3) are determined based on the physical restrictions of the system as discussed in Schneider and Hiller [1995].

For the collision avoidance of obstacles in the environment n_p proximity sensors give the corresponding distance vectors $\boldsymbol{d}_i$ ($d_i = \|\boldsymbol{d}_i\|$, $\boldsymbol{n}_i = \frac{\boldsymbol{d}_i}{\|\boldsymbol{d}_i\|}$). A penetration depth d_0 is defined to protect each obstacle. Based on a nonlinear potential function [Khatib 1986] a repulsive force $\boldsymbol{p}_{ext}$ can be calculated, which is added to the vector $\boldsymbol{p}$ of (Eq. 3).

$$\boldsymbol{p}_{ext} = \sum_{i=0}^{n_p} \boldsymbol{J}_{tcp}^T\,(\kappa_{d_i}\,\boldsymbol{n}_i), \quad (4)$$

$$\kappa_{d_i} = \begin{cases} \kappa_i \left(\frac{1}{d_i} - \frac{1}{d_0}\right) \frac{1}{d_i^2} & ; d_i < d_0 \\ 0 & ; d_i \geq d_0 \end{cases}$$

3 Motion Control of the Tool Center Point

In general, the operator should be able to specify TCP motion using a control device such as a joystick, but in some cases exact positioning and avoiding collisions between the TCP and obstacles would be too difficult for the operator. In these situations the TCP-path is calculated off-line, taking into consideration global geometric information of the environment. Therefore an artifical elastic band [Khatib and Quinlan 1993] is included in the inverse kinematics (Eq. 3) of the controller to avoid collisions of the TCP. In the first step, the discrete data which are supplied by the global path planner have to be smoothed with splines. In the second step a time parameterization is necessary, taking into account the natural constraints of the manipulator e.g. maximum rates of velocity and acceleration.

3.1 The Principle of the Elastic Band

The construction of such an elastic band is based on three dimensional end-effector positions (nodes) which are calculated with a global path planner. The interaction between a node and its neighbors is implemented on a force level. To model the contraction of the elastic band internal contraction forces are introduced, which are based on potential spring forces. The corresponding spring potential, with spring constant c_{int}, of the whole band can be written:

$$P_{int}(\boldsymbol{r}_1, \ldots, \boldsymbol{r}_m) := c_{int} \sum_{i=1}^{m-1} ||\boldsymbol{r}_{i+1} - \boldsymbol{r}_i|| , \quad (5)$$

where $\boldsymbol{r}_i$, $i = 1, \ldots, m$ represents the vector from the inertia frame, $\mathcal{K}_I$, to the nodes, i (Fig. 3). Derivation of the spring potential with respect to $\boldsymbol{r}_i$ yields the spring forces, $\boldsymbol{f}_{int,\,i}$, at each node i:

$$\boldsymbol{f}_{int,\,i} = -c_{int} \left(\frac{\boldsymbol{r}_i - \boldsymbol{r}_{i-1}}{||\boldsymbol{r}_i - \boldsymbol{r}_{i-1}||} + \frac{\boldsymbol{r}_{i+1} - \boldsymbol{r}_i}{||\boldsymbol{r}_{i+1} - \boldsymbol{r}_i||} \right) . \quad (6)$$

The inertial force $\boldsymbol{f}_{int,\,i}$ guarantees that the tension in the band when it is in equilibrium is equal

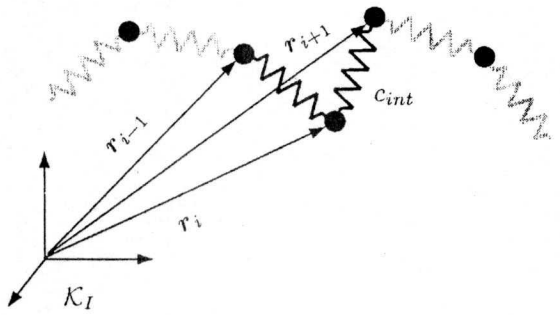

Figure 3: Internal potential forces

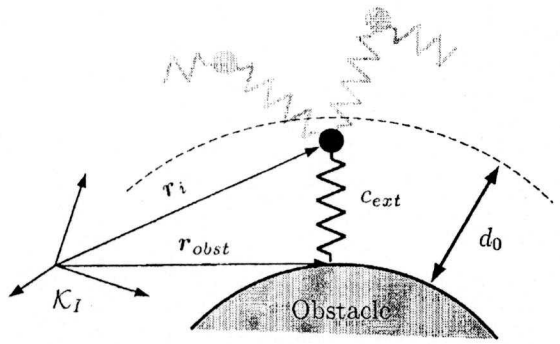

Figure 4: External potential forces

everywhere. The elastic band should also react to obstacles (Fig. 4). Therefore a repulsive nonlinear potential for the whole band is formulated ($\boldsymbol{d}_j = \boldsymbol{r}_j - \boldsymbol{r}_{obst}$):

$$P_{ext}(\boldsymbol{r}_1, \ldots, \boldsymbol{r}_m) := \sum_{j=1}^{m} \begin{cases} \frac{1}{2} c_{ext} \left(d_0 - ||\boldsymbol{d}_j||\right)^2 & ; \; ||\boldsymbol{d}_j|| < d_0 \\ 0 & ; \text{ otherwise} \end{cases} \quad (7)$$

The external potential force is calculated as the negative gradient of the potential P_{ext}:

$$\boldsymbol{f}_{ext,\,i} = \begin{cases} -c_{ext} \left(d_0 - ||\boldsymbol{d}_j||\right) \frac{\boldsymbol{d}_j}{||\boldsymbol{d}_j||} & ; \; ||\boldsymbol{d}_j|| < d_0 \\ \boldsymbol{0} & ; \text{ otherwise} \end{cases} \quad (8)$$

The resulting force acting at a node i is the sum of the internal and the external forces:

$$\boldsymbol{f}_{total,\,i} = \boldsymbol{f}_{ext,\,i} + \boldsymbol{f}_{int,\,i} \; ; \quad i = 1, \ldots, m \quad (9)$$

The new position of the node i can be calculated with a simple equation:

$$\boldsymbol{r}_i^{new} = \boldsymbol{r}_i^{old} + \alpha \boldsymbol{f}_{total,i} \; ; \quad i = 1, \ldots, m \; , \quad (10)$$

where $\alpha \in \mathbb{R}$ is a constant.

3.2 Trajectory of the Tool Center Point – Position

In this section Bezier splines [Bezier 1972] are used to generate continuous, time parameterized, trajectories $\boldsymbol{r}(t)$ from the discrete nodes $\boldsymbol{r}_i$ on the elastic band. The advantage of the Bezier splines is that adding new nodes only results in a local change of the curve in space. A cubic Bezier spline is represented by piecewise cubic parabolic curves, which are smoothly interconnected up to the order of the second differential. With m nodes, $m-1$ curve segments $\boldsymbol{s}_k$ have to be used.

$$\boldsymbol{s}_k(\nu) = \sum_{j=0}^{3} \sum_{k=j}^{3} (-1)^{k+j} \binom{3}{k} \binom{k-1}{k-j} \nu^k \boldsymbol{a}_{j,k}; \quad (11)$$

$$\boldsymbol{a}_{j,k} = \begin{cases} \boldsymbol{b}_{0,k}; & j = 0 \\ \boldsymbol{b}_{j,k} - \sum_{i=0}^{j-1} \boldsymbol{b}_{j-1,k}; & j \neq 0 \end{cases} \quad (12)$$

$$k = 1, \ldots, m-1 \; ; \qquad \nu \in [0, 1]$$

After some simplifications the segment $\boldsymbol{s}_k$ can be represented by the following equation:

$$\boldsymbol{s}_k(\nu) = \boldsymbol{b}_{0,k}(1-\nu)^3 + 3\boldsymbol{b}_{1,k}(1-\nu)^2\nu + 3\boldsymbol{b}_{2,k}(1-\nu)\nu^2 + \boldsymbol{b}_{3,k}\nu^3; \quad \nu \in [0, 1] \quad (13)$$

The Bezier poles $\boldsymbol{b}_{j,k}$ are calculated from the constraint equations such that the interconnections are continuous. For special manipulation tasks the operator may select an approximating or an interpolating spline. The function

$$\nu(\mu) := \mu(m-1) - \mathrm{int}(\mu(m-1)) \qquad (14)$$

is used as the transformation from local to global coordinates, with $\mu \in [0,1]$. This leads to the global Bezier spline $\tilde{\boldsymbol{r}}(\mu) = \boldsymbol{s}_i(\nu(\mu))$, $\frac{i-1}{m-1} \leq \mu < \frac{i}{m-1}$, $i = 1,\ldots,m-1$. In the second step the time parameterization function $\mu(t)$ has to be calculated, while considering the natural constraints. With a given start time t_0 and finish time t_E and $t_0 < t_E$, the function has to fulfil the following conditions:

$$\mu(t_0) = 0; \quad \mu(t_E) = 1; \quad \mu(t) \text{ monotone.} \qquad (15)$$

The trajectory of the TCP in space is given as:

$$\boldsymbol{w}_{tcp,pos}(t) := \tilde{\boldsymbol{r}}(\mu(t)) \quad ; \qquad t \in [t_0, t_E] \qquad (16)$$

The expressions for the velocity and acceleration are:

$$\frac{d}{dt}\boldsymbol{w}_{tcp,pos}(t) = (m-1)\frac{\partial \boldsymbol{s}_i}{\partial \nu}\frac{\partial \mu}{\partial t} \qquad (17)$$

$$\frac{d^2}{dt^2}\boldsymbol{w}_{tcp,pos}(t) = \frac{\partial^2 \boldsymbol{s}_i}{\partial \nu^2}\left((m-1)\frac{\partial \mu}{\partial t}\right)^2 + \frac{\partial \boldsymbol{s}_i}{\partial \nu}(m-1)\frac{\partial^2 \mu}{\partial t^2}, \qquad (18)$$

3.3 Trajectory of the Tool Center Point – Orientation

In general rotary motion is described with rotation parameters. Here, a method for geodetic interpolation is used. Each finite rotation between an initial and final orientation is traceable to a rotation of an angle β around an fixed axis $\boldsymbol{u}$. Such a rotational motion can be described with the rotation tensor:

$$\underline{\underline{T}}(\boldsymbol{u},\beta) = \cos\beta \boldsymbol{I} + \sin\beta\tilde{\boldsymbol{u}} + (1-\cos\beta)\boldsymbol{u}\circ\boldsymbol{u}, \qquad (19)$$

with the skew symmetric matrix $\tilde{\boldsymbol{u}}$ and the dyadic product $\boldsymbol{u}\circ\boldsymbol{u}$. The initial and final orientation of the whole trajectory are represented with transformation matrices ${}^I T_0$ and ${}^I T_E$. The relative rotation matrix ${}^0 T_E$ fulfils the equation:

$${}^0 T_E = ({}^I T_0)^T {}^I T_E = \begin{bmatrix} e_{1,x} & e_{2,x} & e_{3,x} \\ e_{1,y} & e_{2,y} & e_{3,y} \\ e_{1,z} & e_{2,z} & e_{3,z} \end{bmatrix}. \qquad (20)$$

The angular difference, $\Delta\beta$, between both rotations can be calculated as:

$$\cos(\Delta\beta) = \frac{e_{1,x} + e_{2,y} + e_{3,z} - 1}{2}. \qquad (21)$$

The components of the direction vector of the skew axis is calculated as follows. If $\Delta\beta = 0$ then no rotation has to be applied and the skew tensor is equal to the identity tensor, but if $\sin(\Delta\beta) \neq 0$:

$$u_x = \frac{e_{2,z} - e_{3,y}}{2\sin(\Delta\beta)}, \quad u_y = \frac{e_{3,x} - e_{1,z}}{2\sin(\Delta\beta)}, \qquad (22)$$

$$u_z = \frac{e_{1,y} - e_{2,x}}{2\sin(\Delta\beta)}. \qquad (23)$$

If $\Delta\beta = \pm\pi$ the rotation axis is described by:

$$u_x = \pm\sqrt{\frac{e_{1,x}+1}{2}}, \; u_y = \pm\sqrt{\frac{e_{2,y}+1}{2}}, \qquad (24)$$

$$u_z = \pm\sqrt{\frac{e_{3,z}+1}{2}}. \qquad (25)$$

The time dependent transformation matrix of the TCP with respect to the inertia frame can be calculated with the time parameterization $\mu(t)$ given in Eq. (15):

$${}^I T_{tcp}(t) = {}^I T_0 \underline{\underline{T}}(\boldsymbol{u}, \beta(t)) \quad \text{with} \qquad (26)$$

$$\beta(t) := \beta(\mu(t)) = \Delta\beta\mu(t)$$

The rotation vector $\boldsymbol{w}_{tcp,rot}$ can be calculated from ${}^I T_{tcp}$ using a special set of rotation parameters (e. g. Euler angles). For the angular velocities and angular accelerations yields:

$${}_I\boldsymbol{\omega}_{tcp} = \boldsymbol{u}\Delta\beta\dot{\mu}(t), \qquad {}_I\dot{\boldsymbol{\omega}}_{tcp} = \boldsymbol{u}\Delta\beta\ddot{\mu}(t) \qquad (27)$$

4 Collision Avoidance in a Varying Environment

The concepts for collision avoidance in section 2.1 and 3.1 are developed at first for static obstacles (e. g. buildings, trees and high voltage transmission lines). But this concept is also suitable for environments with dynamic obstacles (e. g. an other manipulator in the workspace). In this cases just the parameters of the potential forces have to be modified to react faster to moving obstacles. The penetration depth d_0 of the potential forces has to be increased. This concept is called sensor based collision avoidance.

An alternative can be given by a manual user controlled collision avoidance. This concept is used

in situations, where sensor systems have failed. Therefore a three dimensional simulation model of the manipulator is interconnected with the real system via a client server principle. The update of both systems has to be realized in real time.

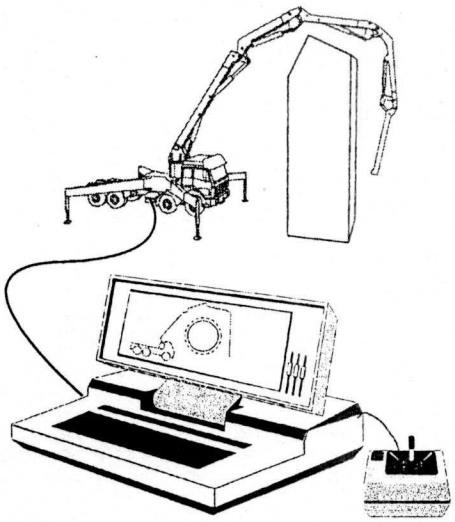

Figure 5: Manual Collision Avoidance

5 Simulation Results

Fig. 6 shows the planned trajectory of the TCP, the moved and additional obstacles, and the shape of the elastic band in the x-y plane. The planned path is given by the global path planner [Frik and Markus 1998] in discrete coordinates. The path represents the shortest path in the joint space (configuration space). It can be seen that the planned path of TCP collides with obstacle 2, if no modification of the path is carried out. In the meantime the obstacle 1 has moved to 1'. The elastic band has to fulfil two important tasks. On the one hand the path has to become smooth to avoid artifical excited vibrations in the system. On the other hand collision free motion has to be guaranteed. The elastic band represented in Fig. 6 fulfils these requirements. In Fig. 7 unified motion control of the redundant d.o.f. and the elastic band are represented. The intermediate configurations (grey) between the initial and final configurations show that collision avoidance of the boom is also guaranteed. Fig. 8 shows the result of the geodetic orientation control of the TCP. It has to be mentioned that the orientation trajectory in the

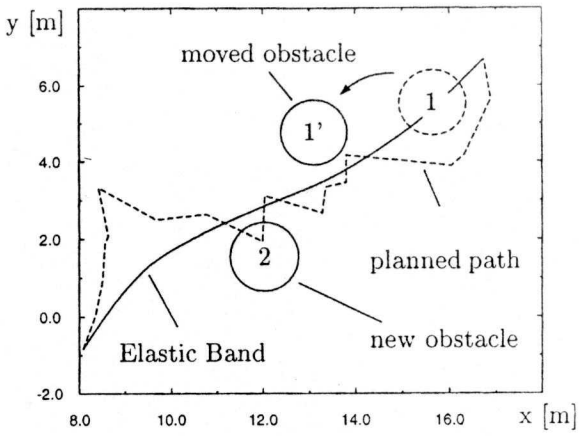

Figure 6: Elastic Band and Obstacles

three dimensional workspace represents the shortest "distance" between the initial and final orientations.

For all simulations the hierarchical control concept of Schneider and Hiller [1996] is applied. An overview of this concept is given in Fig. 9. In a first step the motion control of the TCP gives the nominal vector $\hat{\boldsymbol{w}}_{tcp} = [\boldsymbol{w}_{tcp}^T, \dot{\boldsymbol{w}}_{tcp}^T, \ddot{\boldsymbol{w}}_{tcp}^T]$. The output of the PD-controller and the vector $\boldsymbol{p}$ of the redundant d.o.f. control are used in the inverse kinematics. The forces for the decentralized force controller are calculated with the inverse dynamics of the system. Finally the mechanical system is driven by electro-hydraulic drives.

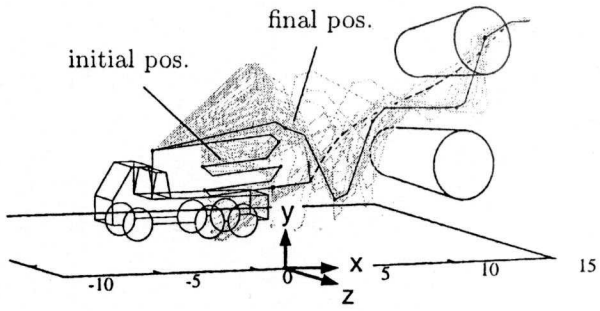

Figure 7: Motion control with collision avoidance

6 Conclusions

The concept for motion control of the TCP and the redundant d.o.f. is an effective framework for the use of path-planner information for collision-free motion in a changing environment. Simula-

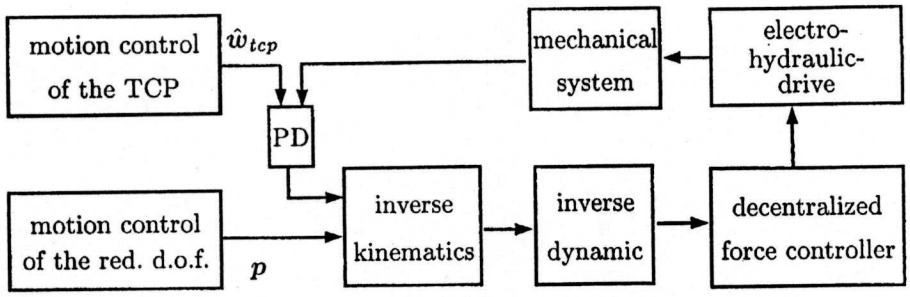

Figure 9: Hierarchical Control Concept

Figure 8: Orientation of the TCP

tion results show that collisions with moved and unexpected new obstacles are also avoidable. For TCP motion control an elastic band is used, where geodetic orientation is considered. Nevertheless further dynamic effects of the system have to be investigated.

References

Bezier, P., editor (1972). *Numerical Control Mathematics and Applications.* New York-London-Toronto.

Frik, M. and Markus, B. (1998). Bestimmung von Zwischenschritten für die Kollisionserkennung von Robotern. In Mennicken, R. and Pfeiffer, F., editors, *ZAMM Zeitschrift für angewandte Mathematik und Mechanik*, volume 78 of *GAMM 97 Annual Meeting, Regensburg, Germany, March 24–27*, pages S387–S388, Berlin. Gesellschaft für angewandte Mathematik und Mechanik, WILEY-VCH.

Khatib, O. (1986). Real–Time Obstacle Avoidance for Manipulators and Mobile robots. *Int. Journal of Robotics Research*, 5:90–98.

Khatib, O. and Quinlan, S. (1993). Elastic bands: Connecting path planning and control. In *Proc. IEEE International Conference on Robotics and Automation*, Atlanta (1993).

Schneider, M. and Hiller, M. (1995). Modelling, simulation and control of a large hydraulically driven redundant manipulator with flexible links. In *Proceedings of the 9th World Congress on Theory of Machines and Mechanisms*, pages 3038–3043, Politecnico di Milano, Italy. IFToMM.

Schneider, M. and Hiller, M. (1996). Vibration suppressing for hydraulically driven large redundant manipulators. In Morecki, A., Bianchi, G., and Rzymkowski, C., editors, *Proceedings of the 11th CISM-IFToMM Symposium on Theory and Practice of Robots and Manipulators (Ro.Man.Sy. '96)*, pages 73–80, Udine, Italy. CISM-IFToMM, Springer-Verlag Wien New York.

Schneider, M., Hiller, M., and Wagner, S. (1995). Dynamic simulation, nonlinear control and collision avoidance of hydraulically driven large redundant manipulators. In Budny, E., McCrea, A., and Szymański, K., editors, *Automation and Robotics in Construction XII*, pages 341–348, 12th ISARC, Warszawa, Poland. Instytut Mechanizacji Budownictwa i Górnictwa Skalnego (IMBiGS), Warszawa, Poland.

Wanner, M. C. (1996). Aircraft washing system skywash. *Advanced Robotics*, 10:415–423.

Whitney, D. E. (1969). Resolved motion rate control of manipulators and human prostheses. MMS-10:47–53.

Woernle, C. (1993). Nonlinear control of constrained redundant manipulators. In Angeles, J., Hommel, G., and Kovacs, P., editors, *Computational Kinematics*, pages 119–128.